Applied and Computational Mechanics 20 (2026) XXX–YYY

Kriging-assisted multi-objective optimization of a wind turbine blade based on fluid-structure interaction analysis

H. I. Abdoulaye[a,*], R. El Maani[a]

[a] *PEME Laboratory, ENSA Khouribga, Sultan Moulay Slimane University, Morocco*

Received 5 March 2026; accepted 24 June 2026

Abstract

This study presents a surrogate-assisted multi-objective framework for a GE 1.5XLE horizontal-axis wind turbine (HAWT) blade based on a one-way fluid-structure interaction (FSI) analysis. The objective is to identify optimal trade-offs between structural weight reduction and dynamic performance by simultaneously minimizing blade mass and maximizing the fundamental natural frequency. Aerodynamic loads are first computed using computational fluid dynamics (CFD) and subsequently transferred to a structural finite element analysis (FEA) model through a one-way FSI coupling. To reduce the computational cost associated with repeated high-fidelity simulations, a Kriging metamodel is constructed using a latin hypercube sampling (LHS) design of experiments. The resulting surrogate model demonstrated high predictive accuracy, with a maximum prediction error below 0.4 %. A multi-objective genetic algorithm (MOGA) is then employed to generate the Pareto optimal set of solutions and to identify the best compromise designs under stress and deformation constraints. The optimal design achieves an approximately 10% reduction in total mass and a 9.1% increase in fundamental frequency compared with the baseline blade, while satisfying all structural requirements. Independent high-fidelity numerical verification confirms the reliability of the proposed framework, with deviations of less than 0.2 %. The proposed FSI-Kriging-MOGA methodology provides an efficient and reliable computational tool for the aeroelastic optimization of wind turbine blades and can be extended to other complex fluid-structure interaction systems.

Keywords: wind turbine blade, multi-objective optimization, fluid-structure interaction, kriging, genetic algorithm

1. Introduction

Renewable energy production stands as a cornerstone of the global energy transition. Among these sources, wind energy has established itself as one of the most mature and competitive, thanks to continuously decreasing costs and improving system performance [4]. Wind turbine blades play a crucial role in this energy conversion process, transforming the wind's kinetic energy into mechanical energy while being subjected to intense aerodynamic and structural loads [6]. Their design must therefore achieve an optimal compromise between aerodynamic efficiency, structural stiffness and fatigue resistance.

The analysis of blade aeroelastic behavior relies on a detailed understanding of fluid-structure interaction (FSI). Hybrid numerical approaches combining computational fluid dynamics (CFD) and finite element analysis (FEA) have emerged as powerful tools for predicting blade deformations, stresses and vibration modes under realistic operating conditions [14]. These coupled models significantly reduce the reliance on costly experimental testing while improving prediction accuracy. Despite their accuracy, high-fidelity FSI simulations remain computationally expensive, particularly when integrated into optimization frameworks. A typical op-

*Corresponding author. Tel.: +212 608 371 286, e-mail: abdoulaye.harounaillou@usms.ac.ma.
https://doi.org/10.24132/acm.2026.1096

timization process may require hundreds or even thousands of numerical evaluations, making direct simulation-based optimization impractical for large-scale wind turbine blades. This limitation becomes even more pronounced in multi-objective optimization problems, where designers seek optimal trade-offs between conflicting objectives such as minimizing structural mass while maximizing stiffness, natural frequencies or fatigue resistance.

To overcome the computational burden associated with repeated numerical analyses, surrogate-based optimization methods have gained considerable attention in recent years [18]. These methods replace expensive numerical simulations with computationally efficient approximation models capable of reproducing the input-output relationships of the original system. Among the available surrogate modeling techniques, kriging has proven particularly effective for highly nonlinear engineering problems due to its interpolation capability, prediction accuracy and built-in uncertainty estimation. When combined with design of experiments (DOE) techniques such as latin hypercube sampling (LHS), kriging enables efficient exploration of complex design spaces while maintaining high predictive fidelity. Simultaneously, evolutionary multi-objective optimization algorithms have become powerful tools for solving engineering design problems involving conflicting objectives and nonlinear constraints. Unlike traditional gradient-based methods, multi-objective genetic algorithms (MOGA) can efficiently explore large and discontinuous design spaces while generating a complete Pareto optimal set of solutions. This capability is particularly valuable in wind turbine blade design, where improving one performance criterion often leads to the deterioration of another [3, 13, 16].

Several studies have investigated structural optimization, aeroelastic analysis and surrogate-based design methodologies for wind turbine blades. Recent works have focused on aerodynamic shape optimization, composite material tailoring, uncertainty quantification and multidisciplinary design optimization [7, 11]. Although significant progress has been achieved, relatively few studies have proposed an integrated framework that combines high-fidelity FSI simulations, global sensitivity analysis, kriging metamodeling and evolutionary multi-objective optimization within a unified workflow for utility-scale wind turbine blades. Furthermore, the identification of influential aeroelastic parameters before surrogate construction remains insufficiently explored despite its potential to improve both model accuracy and computational efficiency.

Motivated by these challenges, the present study proposes an integrated FSI-Kriging-MOGA framework for the multi-objective optimization of a GE 1.5XLE horizontal-axis wind turbine blade. The methodology combines high-fidelity one-way FSI simulations performed in ANSYS Fluent and ANSYS Mechanical with global sensitivity analysis, latin hypercube sampling, kriging surrogate modeling, and multi-objective genetic algorithm optimization to simultaneously minimize blade mass and maximize the fundamental natural frequency while satisfying structural constraints on maximum deformation and equivalent stress. The proposed study enables the identification and ranking of the most influential aerodynamic and structural parameters governing the response of a utility-scale wind turbine blade, thereby reducing the dimensionality of the optimization problem. A high-accuracy kriging surrogate model is constructed and validated to reproduce FSI responses with very low prediction errors, significantly improving computational efficiency compared with direct high-fidelity simulations. The framework is subsequently employed to generate a Pareto optimal set of blade designs that explicitly quantifies the trade-off between structural weight reduction and dynamic stiffness. Finally, the robustness and reliability of the proposed methodology are confirmed through independent high-fidelity numerical simulations of the optimal design. This provides a practical and reliable decision-support tool for the preliminary design and optimization of large-scale composite wind tur-

bine blades while substantially reducing the computational cost associated with conventional simulation-based optimization approaches.

This article is structured as follows: Section 2 introduces the fundamentals of multi-objective optimization and MOGA. Section 3 describes the numerical methodology in detail. Section 4 presents the simulation and optimization results. Finally, Section 5 synthesizes the main conclusions of this study.

2. Multi-objective optimization method

MOGA implemented in the goal driven optimization (GDO) module is a hybrid approach derived from the well-known NSGA-II framework, incorporating a controlled elitism strategy. It is capable of handling a wide range of design variables. Pareto dominance is evaluated using an efficient fast non-dominated sorting procedure, which significantly reduces computational cost compared with classical Pareto ranking techniques. Constraint treatment follows the same dominance-based philosophy applied to the objective functions, eliminating the need for penalty terms or Lagrange multipliers. As a result, feasible solutions are systematically assigned higher priority than infeasible ones.

The concept of Pareto dominance is fundamental in multi-objective optimization, particularly when objectives and constraints conflict. Unlike single-objective problems, there is generally no unique solution that simultaneously optimizes all criteria. The Pareto approach instead identifies a set of non-dominated solutions, where any improvement in one objective necessarily leads to the degradation of at least one other.

A point $x' \in X$ is said to be Pareto optimal for the problem if there is no other vector $x \in X$ such that

$$f_i(x) \leq f_i(x^*),\ i = 1, \ldots, k, \tag{1}$$

$$f_i(x) < f_i(X^*). \tag{2}$$

This definition formalizes the idea that a solution is optimal if no criterion can be improved without deteriorating others. The set of Pareto optimal solutions forms the Pareto front. While traditional algorithms often guarantee only local optimality, evolutionary methods such as MOGA, incorporating global Pareto filters, enable efficient approximation of the global Pareto front for complex problems.

The solutions belonging to the leading Pareto front are stored internally in a dedicated archive that is separate from the active population undergoing evolution. This strategy preserves previously identified Pareto optimal patterns and prevents them from being altered by subsequent generations. The level of selection pressure, and thus the degree of elitism, can be adjusted through the maximum allowable Pareto percentage parameter, which helps mitigate the risk of premature convergence. The optimization procedure is organized into a systematic six-step workflow:

- *Step 1: Initialization of the MOGA population.* The algorithm begins by evaluating an initial population of candidate solutions.
- *Step 2: Generation of a new population.* A new population is created through genetic operators such as crossover and mutation. From the second iteration onward, each population is evaluated once it reaches the predefined number of samples specified by the number of samples per iteration setting.
- *Step 3: Update of design variables.* The design points corresponding to the newly generated population are updated accordingly.

- *Step 4: Convergence assessment.* The algorithm checks whether convergence has been achieved. Convergence is declared when either the maximum allowable Pareto percentage or the convergence stability percentage threshold is satisfied. If convergence is not attained, the process proceeds further.
- *Step 5: Evaluation of stopping conditions.* In the absence of convergence, the algorithm verifies whether predefined stopping criteria are met. If the maximum number of iterations is reached, the optimization terminates without convergence; otherwise, the algorithm returns to the population generation stage.
- *Step 6: Termination of the optimization process.* Steps 2 through 5 are iteratively repeated until either convergence is achieved or a stopping condition is triggered, at which point the optimization process ends.

3. Kriging metamodel

The construction of a response surface (or metamodel) involves using mathematical methods to fit the points of a design of experiments (DOE). Various construction methods exist, such as second-order polynomials, kriging, non-parametric regression or neural networks.

The kriging algorithm is particularly well-suited for highly nonlinear responses, as it offers improved prediction quality by accounting for higher-order variations in the output parameters. It is an accurate multidimensional interpolation that combines [9, 19]

- a polynomial model, providing a 'global' trend across the design space;
- local deviations, modeled by a Gaussian process, which enable kriging to exactly interpolate the points of DOE.

Kriging allows for adaptive refinement for continuous input parameters. Its efficiency stems from the ability of its internal error estimator to improve the response surface by iteratively generating new refinement points in areas where uncertainty is the highest. This self-refining capability, coupled with exact data interpolation, often makes the Kriging model more reliable than a classical polynomial model.

Kriging postulates a combination of a polynomial model plus departures of the form given by

$$y(x) = f(x) + Z(x), \tag{3}$$

where $y(x)$ denotes the unknown response function to be modeled, $f(x)$ represents a polynomial function of the input variable x, and $Z(x)$ corresponds to a realization of a Gaussian random process with zero mean, variance σ^2, and a non-vanishing covariance structure. The polynomial component $f(x)$ plays a role analogous to that used in response surface methodologies, serving as a global approximation of the design domain.

Although $f(x)$ captures the overall trend of the response across the design space, the stochastic term $Z(x)$ accounts for *local* variations, enabling the Kriging model to exactly reproduce the available sample observations. The covariance structure associated with $Z(x)$ is defined as follows:

$$\mathrm{Cov}\left[Z(x^i), Z(x^j)\right] = \sigma^2\, \mathbf{R}\Big(\left[r(x^i, x^j)\right]\Big), \tag{4}$$

where $\mathbf{R}$ denotes the correlation matrix and $r(x^i, x^j)$ represents the spatial correlation between the response values at any two sample locations x^i and x^j among the N available data points. The matrix $\mathbf{R}$ is an $N \times N$ symmetric and positive definite, with unit entries along its main diagonal. The correlation between two sample points is modeled using a Gaussian correlation

function of the form

$$r(x^i, x^j) = \exp\left(-\sum_{k=1}^{M} \theta_k \left|x_k^i - x_k^j\right|\right), \tag{5}$$

where M is the number of design variables, θ_k are the unknown parameters used to fit the model, and x_k^i and x_k^j are the sample points of the k-th component.

Several statistical indicators are evaluated using the data points employed in the development of the response surface model, including the following:

- *Coefficient of determination (R^2):* This metric represents the proportion of the total variance of the output response that is captured by the response surface regression model. It is defined as the ratio between the variance explained by the model and the overall variance of the data, with an ideal value equal to 1,

$$R^2 = 1 - \frac{\sum_{i=1}^{N}(y_i - \hat{y}_i)^2}{\sum_{i=1}^{N}(y_i - \bar{y})^2}, \tag{6}$$

  where y_i denotes the actual value of the output parameter at the i-th sampling point, $\hat{y}_i$ corresponds to the predicted value obtained from the regression model at the same point, $\bar{y}$ is the arithmetic mean of the observed output values, and N represents the total number of sampling points.
- *Relative average absolute error (RAAE)*: This metric is the average of the residuals relative to the standard deviation of the actual outputs. The best value is 0 %. In general, the closer the value is to 0 %, the better the quality of the response surface. The relative average absolute error is mathematically represented as

$$\mathrm{RAAE} = \frac{1}{\sigma_y}\frac{1}{N}\sum_{i=1}^{N}\left|y_i - \hat{y}_i\right|, \tag{7}$$

  where σ_y represents the standard deviation of the values y_i.

4. Integrated FSI-Kriging-MOGA optimization frameworks

The proposed optimization framework combines high-fidelity FSI simulations, surrogate modeling, and MOGA within a unified computational workflow illustrated in Fig. 1. The methodology is organized into three sequential stages:

- *Physical modeling:* First, CFD simulations are performed using ANSYS Fluent to model airflow around the blade. The one-way FSI approach is implemented by transferring computed aerodynamic forces to the structural model in ANSYS Mechanical for FEA, without feedback to the fluid solver. This method provides an efficient and reliable evaluation, delivering accurate predictions of mechanical stresses, deformations and natural frequencies.
- *Metamodeling:* Second, a validated Kriging metamodel is constructed from DOE to accurately approximate the numerical responses while significantly reducing computational cost.
- *Multi-objective optimization:* Finally, MOGA is applied to this metamodel, serving as a fast response surface, to iteratively generate the Pareto front, thereby identifying the complete set of optimal solutions for blade design.

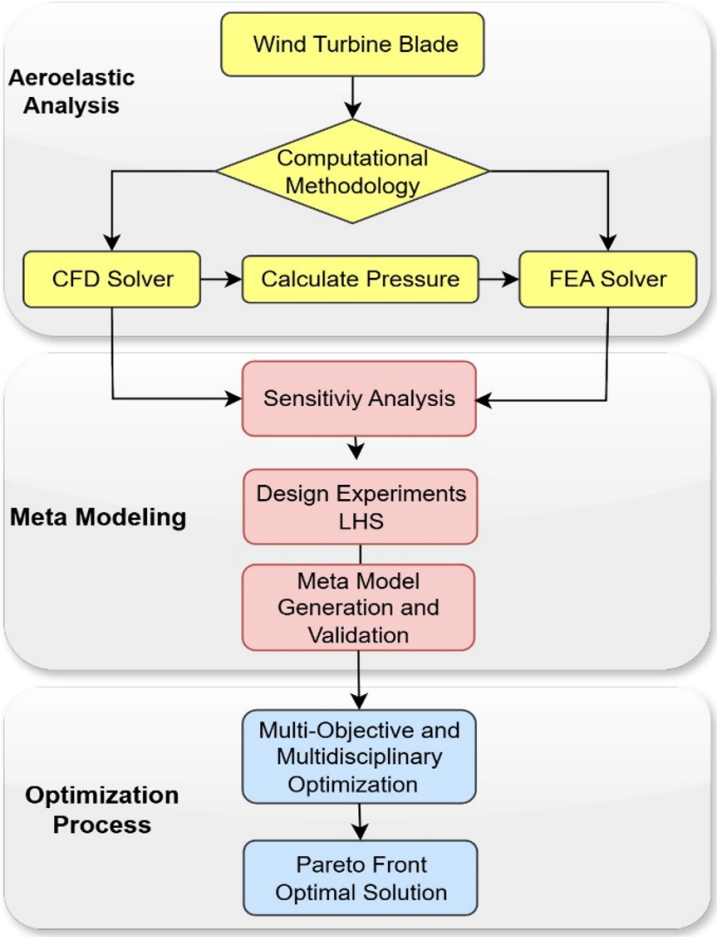

Fig. 1. Integrated methodology workflow for wind turbine blade optimization

5. Numerical simulations

5.1. CFD investigation

The numerical setup represents a full-scale industrial wind turbine blade with a span of 43.2 m, corresponding to the GE 1.5XLE configuration. The computational domain is composed of two coaxial cylindrical regions aligned with the z-axis: an upstream inlet located 90 m ahead of the rotor plane with a radius of 120 m, and a downstream outlet placed 180 m behind the rotor with a radius of 240 m.

The flow field is simulated using ANSYS Fluent under incompressible conditions, with air entering the domain along the negative z-direction at a uniform velocity of 12 m/s. The blade is subjected to a rotational speed of -2.22 rad/s (approximately 21 rpm), which corresponds to the optimal tip-speed ratio (TSR) of 8. The negative sign indicates clockwise rotation in accordance with the right-hand rule adopted in ANSYS Fluent. This rotational direction is physically consistent with the imposed wind direction and typical upwind wind turbine operation. International standard atmosphere (ISA) conditions are assumed, with a temperature of 15 °C and an ambient pressure of 1 atm. As presented in Fig. 2, the inlet imposes a uniform velocity with 5% turbulence intensity and a turbulent viscosity ratio of 10, while the outlet is set to 1 atm. The blade surface is treated as a no-slip wall, and two periodic interfaces (Periodic 1 and Periodic 2) are used to reduce the domain size while preserving flow symmetry.

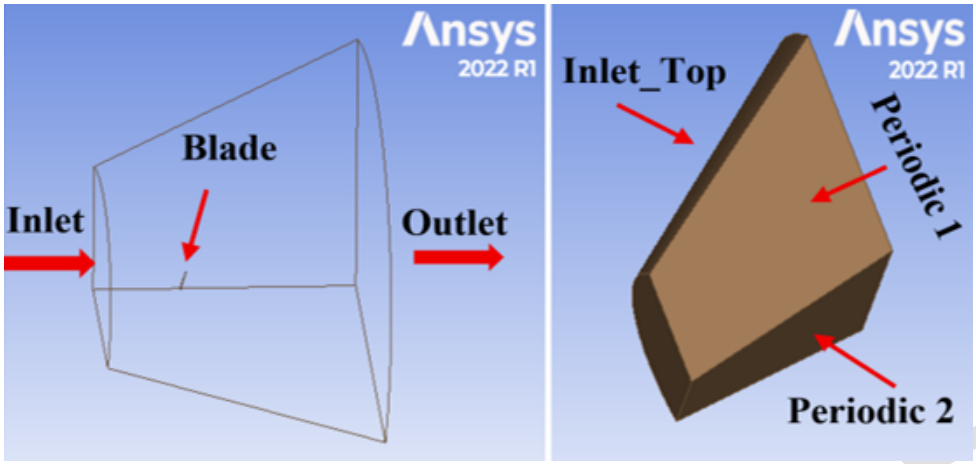

Fig. 2. Computational domain geometry and boundary conditions for the CFD simulation

The mesh was generated using tetrahedral elements. The *Advanced size function* was set to *Proximity and curvature* to optimize the resolution of local curvatures and geometrically complex regions. A *Match control* was applied to the periodic faces to ensure node alignment relative to the axis of rotation.

An element size of 0.05 m was imposed on the blade surface. To accurately capture velocity gradients near the wall, an inflation layer refinement (15 layers, growth rate of 1.2) was integrated. The first layer height was set to 10^{-6} m to ensure that $y^+ \leq 1$, an essential condition for fully exploiting the accuracy of the shear stress transport (SST) k–ω turbulence model. Finally, a sphere of influence with a radius of 50 m, centered on the blade, was defined with an element size of 1 m to enhance the flow field resolution in the immediate vicinity, as mentioned in Fig. 3. This spatial discretization setup resulted in a final mesh comprising 2 424 399 nodes and 8 802 479 elements.

For turbulence modeling, the SST model was selected as it combines the advantages of the k–ε model in the free stream with the k–ω model near the walls. By introducing a cross-diffusion term and accounting for the transport of turbulent shear stress, the SST model significantly improves the prediction of adverse pressure gradients and flow separation on the blade

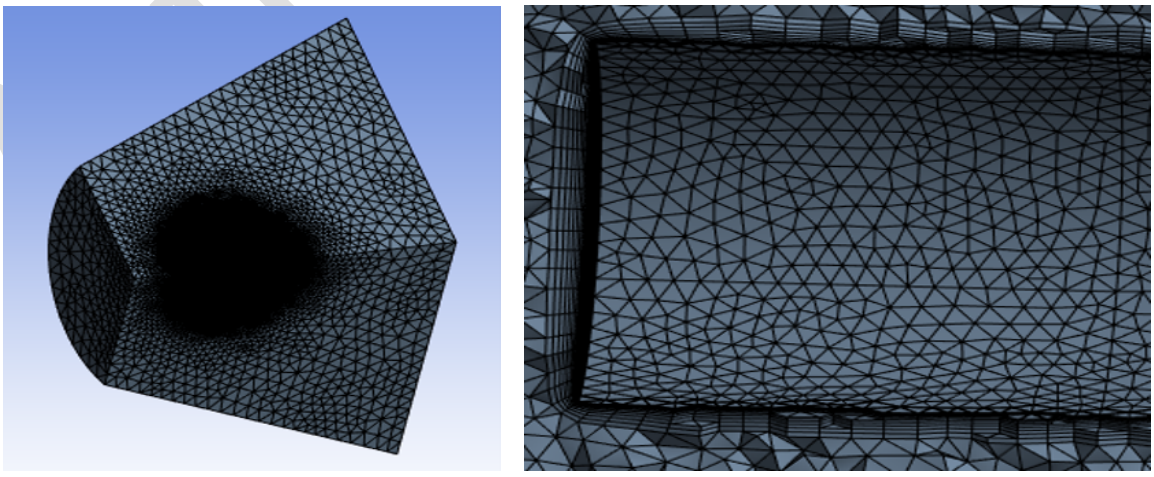

Fig. 3. Computational mesh of the fluid domain (*left*) with a detailed view at the blade vicinity (*right*)

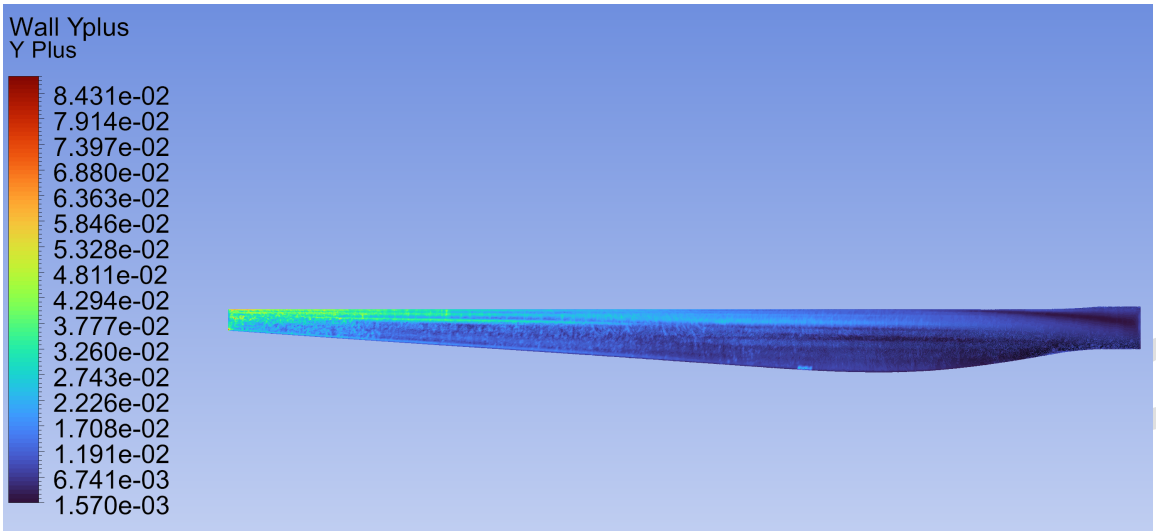

Fig. 4. Distribution of y^+ on the blade surface, ensuring viscous sublayer resolution for the SST k–ω turbulence model

surface. These capabilities are essential for accurately capturing pressure distributions in the subsonic regime [1, 8].

A pressure-based solver was employed to handle the incompressible nature of the flow in steady-state mode. The coupled scheme was chosen for its robustness and accelerated convergence. The maximum number of iterations was set to 1 500, with convergence validated by reaching a residual tolerance of 10^{-6}. This was further confirmed by the stabilization of the integral static pressure on the blade surfaces, monitored via surface reports in ANSYS Fluent.

To ensure mesh-independent results, a convergence study was performed with a focus on boundary layer resolution through the dimensionless wall distance y^+. As shown in Fig. 4, the $y^+ \leq 1$ criterion is fulfilled across the entire blade, confirming the adequate capture of the viscous sublayer required by the SST k–ω turbulence model. Additionally, the power coefficient C_p, which is a key parameter for evaluating the overall performance of a wind turbine, was utilized to further validate the aerodynamic accuracy of the numerical model. The coefficient C_P obtained from the high-fidelity CFD model was compared with the numerical results derived from the blade element momentum (BEM) theory [1]. The BEM model predicts a power coefficient of 0.30, while the 3D CFD simulation yields a value of 0.31. These results demonstrate an exceptional agreement between both numerical approaches. This excellent alignment, combined with the grid independence study, definitively validates both the spatial discretization quality and the robustness of the CFD model based on the SST turbulence closure.

5.2. FEA investigation

In this section, the mathematical model is based on shell theory, an extension of the Euler-Bernoulli beam theory, adapted for thin structures subjected to complex loading conditions, as is the case for wind turbine blades.

The orthotropic composite materials, used in the model and presented in Table 1, are representative of the properties employed in the manufacture of modern wind turbine blades, selected for their excellent strength-to-weight ratio. The modeling incorporates two distinct thicknesses according to the structural regions of the blade. The external surface features a thickness that varies linearly from 0.1 m at the root to 0.005 m at the tip. As for the internal spar, its thickness

Table 1. Material properties (orthotropic composite) [5]

Property	Value
Density [kg/m^3]	1 550
Elastic modulus X [Pa]	1.1375×10^{11}
Elastic modulus Y [Pa]	7.583×10^9
Elastic modulus Z [Pa]	7.583×10^9
Poisson's ratio XY [–]	0.37
Poisson's ratio YZ [–]	0.32
Poisson's ratio XZ [–]	0.35
Shear modulus XY [Pa]	5.446×10^9
Shear modulus YZ [Pa]	2.964×10^9
Shear modulus XZ [Pa]	2.964×10^9

gradually decreases from 0.1 m near the root to 0.03 m at the tip.

A quadrilateral mesh type was specifically applied to the external surface, which is recommended for FEA to improve result quality in critical areas. As presented in Fig. 5 (left), the element size was uniformly set to 0.05 m across the entire blade using the sizing option, ensuring a good compromise between numerical accuracy and computational cost. A rotational velocity of -2.22 rad/s about the z-axis, a fixed support at the blade root to simulate its attachment, and the activation of the 'large displacement' option to account for nonlinear effects were applied. The pressure obtained from the CFD study is imported and applied to the external blade surface, Fig. 5 (right).

Based on the analysis of the deformation and stress contours presented in Fig. 6, the maximum deformation of the blade reaches 0.5645 m, and the maximum stress reaches 38.78 MPa. These values remain below the allowable stress of the material, confirming that the static performance meets the design requirements. This substantial safety margin indicates significant

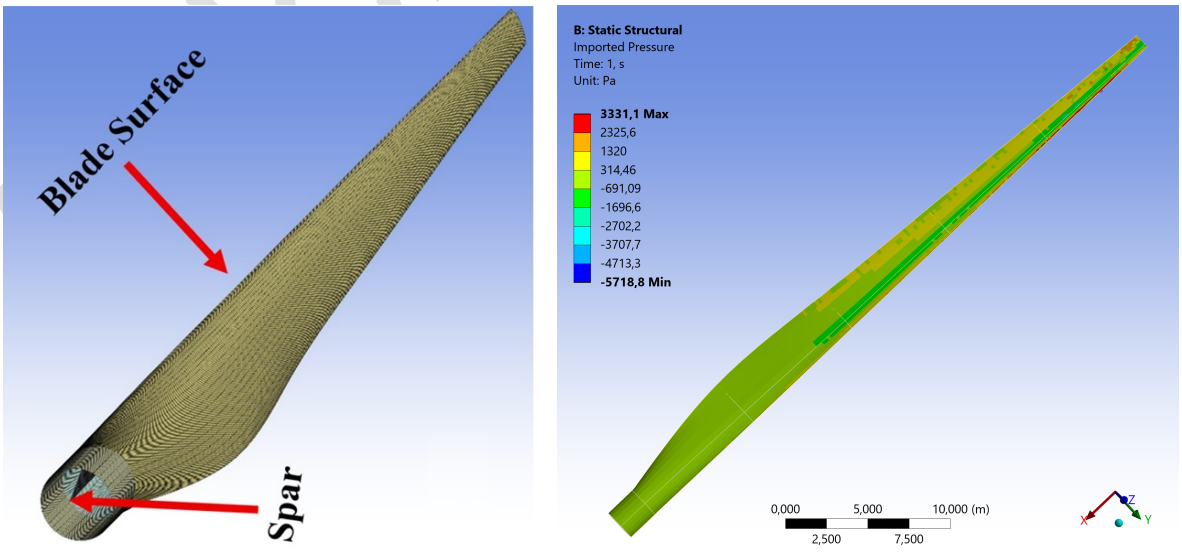

Fig. 5. Structural mesh configuration (*left*) and imported aerodynamic pressure loading (*right*)

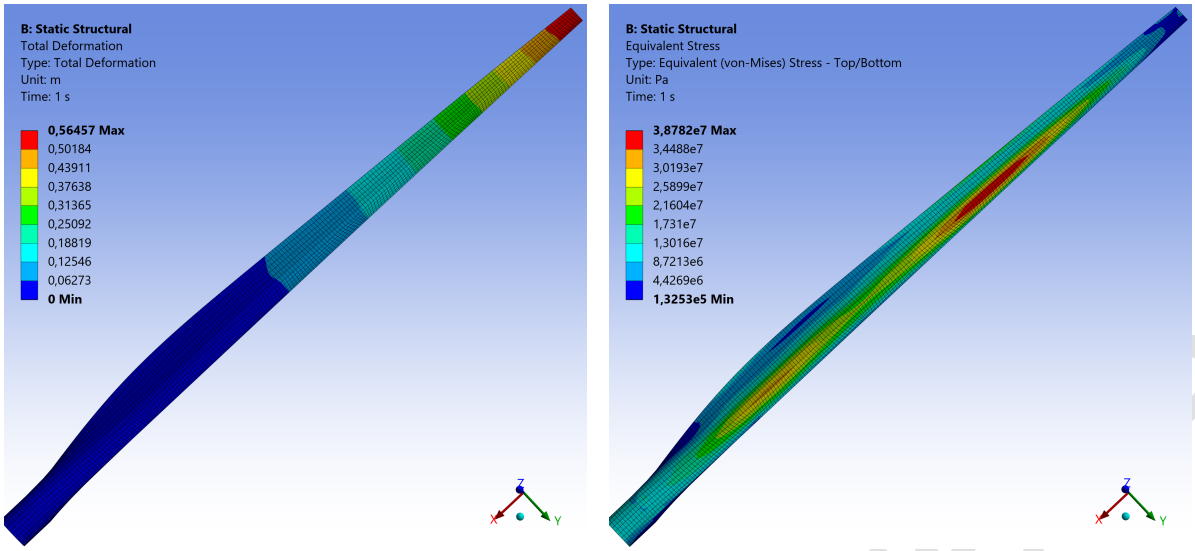

Fig. 6. Structural response: blade total deformation (*left*) and von Mises stress distribution (*right*)

optimization potential for weight reduction of the structure.

The modal analysis was performed considering the pre-stressed state derived from the static analysis (including centrifugal forces and CFD aerodynamic loads), thus accounting for the stress stiffening effect induced by rotation. The natural frequencies for the first six modes are presented in Table 2. The fundamental frequency of the first mode is found to be insufficient, posing a critical risk of resonance with cyclic aerodynamic excitations. This limited dynamic stiffness necessitates a structural optimization to maximize the first mode frequency while minimizing the total blade mass.

Table 2. Modal analysis results: natural frequencies and vibration modes

Order	Natural frequency [Hz]
1	1.6694
2	3.441
3	4.4317
4	7.9085
5	9.3277
6	11.793

5.3. MOGA-based kriging

5.3.1. Sensitivity analysis

Several methods exist for generating calculation points or design points, such as the central composite design and the Box-Behnken design. The latin hypercube sampling (LHS) method was selected for its ability to capture the structural and aerodynamic non-linearities characteristic of blades. It is a more advanced and efficient form of the Monte Carlo analysis methods and is one of the most widely used methods in experimental design. It does not impose a strict mathematical relationship between the number of points N and the number of variables k.

Table 3. Design variables range and bounds for optimization

Variable	Initial value	Lower limit	Upper limit
Fluid density [kg/m^3]	1.225	1.1025	1.3475
Flow velocity [m/s]	12	10.8	13.2
Rotational speed [rad/s]	2.22	1.998	2.442
Material density [kg/m^3]	1 550	1 395	1 705
Young's modulus X [Pa]	1.1375×10^{11}	1.0238×10^{11}	1.2513×10^{11}

In the present study, the number of influential input parameters is $k = 5$. To ensure dense and reliable sampling, an LHS experimental design was generated with $N = 50$ points. Although LHS does not impose a strict mathematical relationship between N and k, an empirical rule $N = 10k$ is proposed for LHS when used with kriging for sensitivity analysis [2, 15]. This ensures sufficient sampling for the complex non-linearities of the aeroelastic problem and aims to achieve exceptional metamodel quality.

Before proceeding with the construction of the metamodel, it is essential to identify the most influential input parameters on the studied responses. This preliminary screening step is crucial in any probabilistic design approach, as it makes it possible to significantly reduce the dimensionality of the design space, thereby optimizing computational complexity while ensuring the physical representativeness of the results.

The analysis considered all properties influencing the FSI coupling, including fluid parameters (fluid velocity, fluid rotational speed, fluid density and viscosity) and structural parameters (blade rotational speed, material density, Young's moduli, Poisson's ratios, shear moduli of the composites). The fluid rotational speed and the blade rotational speed were merged into a single parameter. The monitored output parameters were the total mass, the maximum displacement, the maximum equivalent stress, and the first natural frequency.

A global sensitivity analysis was conducted with a relevance threshold of 0.2. The results showed that only five parameters (rotational speed, fluid velocity, material density, fluid density, and Young's modulus X) exert a significant influence (relevance greater than 0.9) on the output responses (maximum displacement, total mass, and fundamental frequency). Other parameters, including the Poisson's ratios, shear moduli, Young's moduli (Y and Z), and fluid viscosity, exhibited a relevance lower than 0.16 and a R^2 contribution below 0.15 %. They were therefore excluded from the optimization to reduce the problem's dimensionality without compromising the accuracy of the surrogate model.

This hierarchy is supported by Fig. 7, which illustrates the ranking of variables by sensitivity index. The dominance of the five identified parameters is clearly observed. Consequently, these five key variables will be the only input parameters considered in the multi-objective optimization process. Their variation ranges are presented in Table 3.

To illustrate the extent of the design space explored using the LHS method, Table 4 presents a sample of the first eight computation points used for the metamodel construction.

5.3.2. Metamodeling validation

The metamodel in this study is constructed using kriging, a method for which the LHS experimental design is particularly well-suited. The selected configuration of 50 points for $k = 5$ variables follows the empirical recommendation $N = 10k$ by Loeppky et al. [15] and Jones et

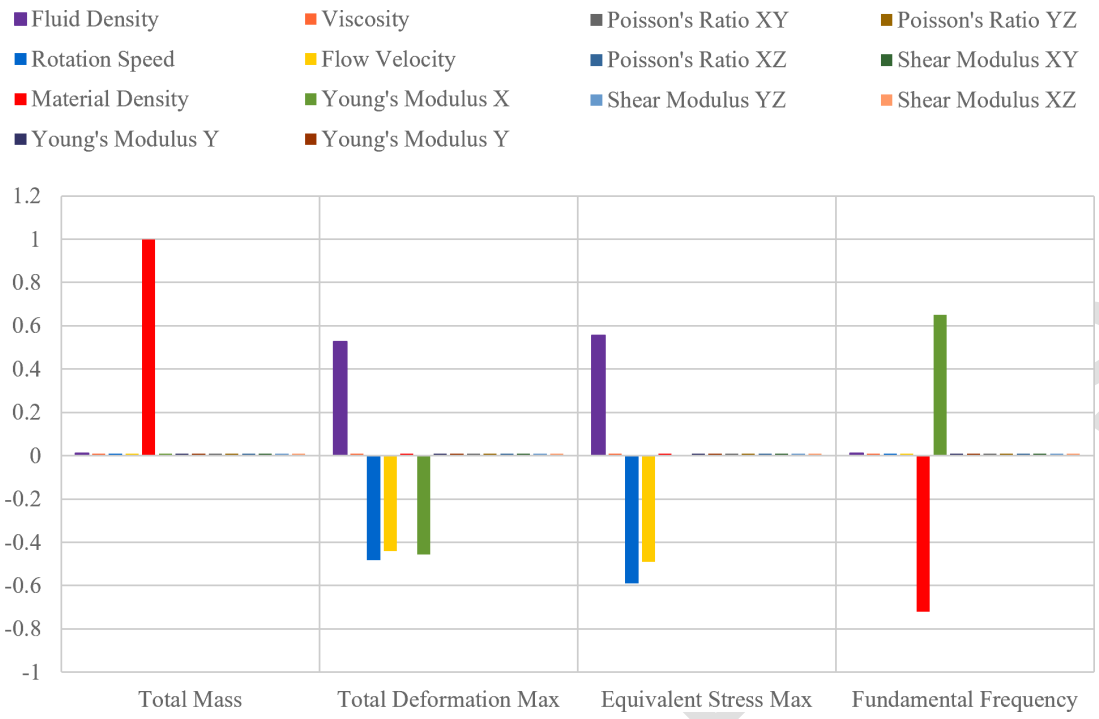

Fig. 7. Global sensitivity analysis of input parameters

Table 4. Sample of first eight LHS design points (P – design points, ϱ_{fluid} – fluid density, ω – rotational speed, v – fluid velocity, ϱ_{mat} – material density, E_X – Young's modulus X, M_{total} – total mass, $D_{\max}$ – maximal total deformation, $\sigma_{\max}$ – maximal equivalent von Mises stress, f_f – fundamental frequency)

P	ϱ_{fluid} [kg/m^3]	ω [rad/s]	v [m/s]	ϱ_{mat} [kg/m^3]	E_X $\times 10^{11}$[Pa]	M_{total} [kg]	$D_{\max}$ [m]	$\sigma_{\max}$ $\times 10^{7}$[Pa]	f_f [Hz]
1	1.1932	2.41092	10.872	1416.7	1.0897	333.3688	0.54681	3.6810	1.7194
2	1.2373	2.1534	12.216	1447.7	1.0351	340.6635	0.61240	3.8011	1.6509
3	1.1099	2.0646	12.984	1559.3	1.1125	366.9245	0.51941	3.4554	1.6396
4	1.2128	2.18004	10.920	1683.3	1.0761	396.1034	0.52389	3.4521	1.5667
5	1.1197	2.33988	12.792	1615.1	1.1944	380.0550	0.55188	3.9903	1.6801
6	1.3304	2.30436	11.736	1410.5	1.2217	331.9099	0.58007	4.2834	1.8041
7	1.2079	2.11788	11.016	1515.9	1.1762	356.7119	0.47828	3.4174	1.7051
8	1.3255	2.17116	13.176	1540.7	1.0624	362.5477	0.68274	4.3141	1.6240

al. [12], ensuring adequate coverage of the design space. Other approaches exist in the literature, such as the Gutmann's full factorial ($N = 2^k = 32$ points) [10] or Regis and Shoemaker's ($N = 2(k + 1) = 12$ points) [17] designs.

Fig. 8 compares the measured values with the kriging predictions (featuring a maximum prediction error below 0.4 %), showing perfect alignment along the diagonal, which confirms the model's excellent fit. Since kriging is an exact interpolator on the training points, additional validation is essential to ensure its robustness. Therefore, the performance of kriging was evaluated and compared to that of a neural network metamodel on an external validation set consisting of five additional points not included in the initial DOE, Table 5.

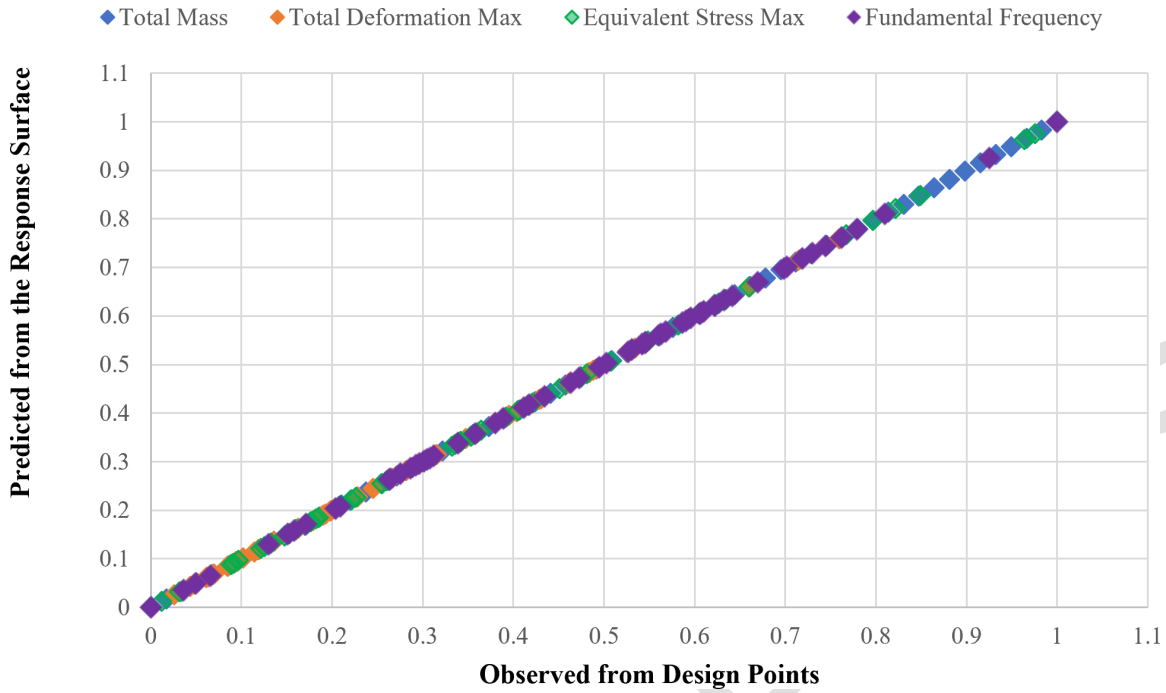

Fig. 8. Kriging metamodel validation between predicted values and numerical results

Table 5. Comparison of predictive performance of kriging and neural network on external validation points

Parameters	Kriging		Neural network	
	R^2 [–]	RAAE [%]	R^2 [–]	RAAE [%]
Max. total deformation $D_{\max}$ [m]	1.000	4.3985	1.000	4.9894
Max. equivalent stress $\sigma_{\max}$ [Pa]	1.000	3.0635	0.999	6.6321
Total mass M_{total} [kg]	1.000	0	0.999	0.4509
Fundamental frequency f_f [Hz]	1.000	0.5987	0.999	2.0500

Both methods exhibit excellent coefficients of determination ($R^2 \geq 0.999$). However, kriging demonstrates superior predictive accuracy, with significantly lower RAAE across all output parameters. For example, for the fundamental frequency, kriging achieves 0.59 % compared to 2.05 % for the neural network; for the maximum equivalent stress, it achieves 3.06 % versus 6.63 %. Regarding total mass, kriging achieves a perfect prediction (RAAE $= 0\,\%$), while the neural network shows a slight error of 0.45 %.

This optimal performance of kriging, achieved with sampling that conforms to theoretical recommendations, validates both the method and the chosen sampling strategy for this fluid-structure interaction problem.

5.3.3. Multi-objective optimization results

The optimization phase aims to determine the optimal design properties for the wind turbine blade, considering the trade-offs between structural and dynamic performance. The optimization problem is formulated as a constrained multi-objective optimization and is implicitly defined as follows:

- *Objectives:*

$$\begin{cases} \min f_1(x) = M_{\text{total}}, \\ \max f_2(x) = f_f. \end{cases}$$

The fundamental frequency f_f and the total mass M_{total} are linked by the classical relationship $f_f \propto \sqrt{k/M_{\text{total}}}$. Consequently, a modification in one parameter directly affects the other. The joint optimization of these objectives aims to design a blade that is both lightweight and sufficiently stiff to avoid resonance. The algorithm achieves this by eliminating 'dead mass'—superfluous material that does not contribute to mechanical performance—while reinforcing critical bending directions. Specifically, it identifies regions where the composite layup thickness is redundant relative to local stresses, allowing for mass reduction while enhancing the specific stiffness of the structure.

- *Subject to the following safety and operational constraints:*

$$\begin{cases} g_1(x) : D_{\max} \leq 0.6\,\text{m}, \\ g_2(x) : \sigma_{\max} \leq 45\,\text{MPa}, \end{cases}$$

where $D_{\max} = 0.5654\,\text{m}$ and $\sigma_{\max} = 38.78\,\text{MPa}$ represent the reference values obtained by simulation before optimization. The choice of constraint values is based on established practices for wind turbine blade design. The displacement limit of 0.60 m represents a controlled 6% increase over the reference value, providing an optimization margin while maintaining geometric integrity and aerodynamic performance; margins of this magnitude are typical in parametric design studies. The stress limit of 45 MPa incorporates a safety factor compliant with standards for glass fiber reinforced polymer (GFRP) composites, where factors of 1.15 to 1.25 are commonly applied to ultimate loads to account for fatigue and loading uncertainties. These conservative margins also help to compensate for the numerical uncertainties inherent in large-scale multiphysics simulations.

The optimization was performed in MATLAB using MOGA. The process begins with an initial population of 100 individuals generated via LHS, ensuring a uniform exploration of the design space.

The evolutionary dynamics are based on the simulated binary crossover operator and polynomial mutation, with distribution indices set to $\eta_c = 20$ and $\eta_m = 20$, respectively. The mutation probability was defined by the rule $P_m = 1/V$, where $V = 6$ is the number of design variables. Parent selection is carried out by tournament, while the preservation of optimal solutions is ensured by Pareto dominance sorting and the computation of crowding distance to maintain solution diversity. The algorithm was run for 500 generations to identify the global Pareto front, providing a robust trade-off between blade mass and fundamental frequency under constraints on maximum total displacement and maximum equivalent stress.

The analysis of the results is illustrated by the Pareto front presented in Fig. 9. This front represents the set of optimal solutions to the mass-frequency trade-off problem. In accordance with the Pareto principle, none of these solutions can improve one objective without degrading the other. The obtained frontier reveals a favourable trade-off relationship: A significant increase in the fundamental frequency can be achieved at the cost of a moderate increase in mass.

The selected optimal candidate (Table 6) demonstrates a notable improvement over the original design. The total mass is reduced by 9.999 % (from 364.7361 kg to 328.2644 kg) while the

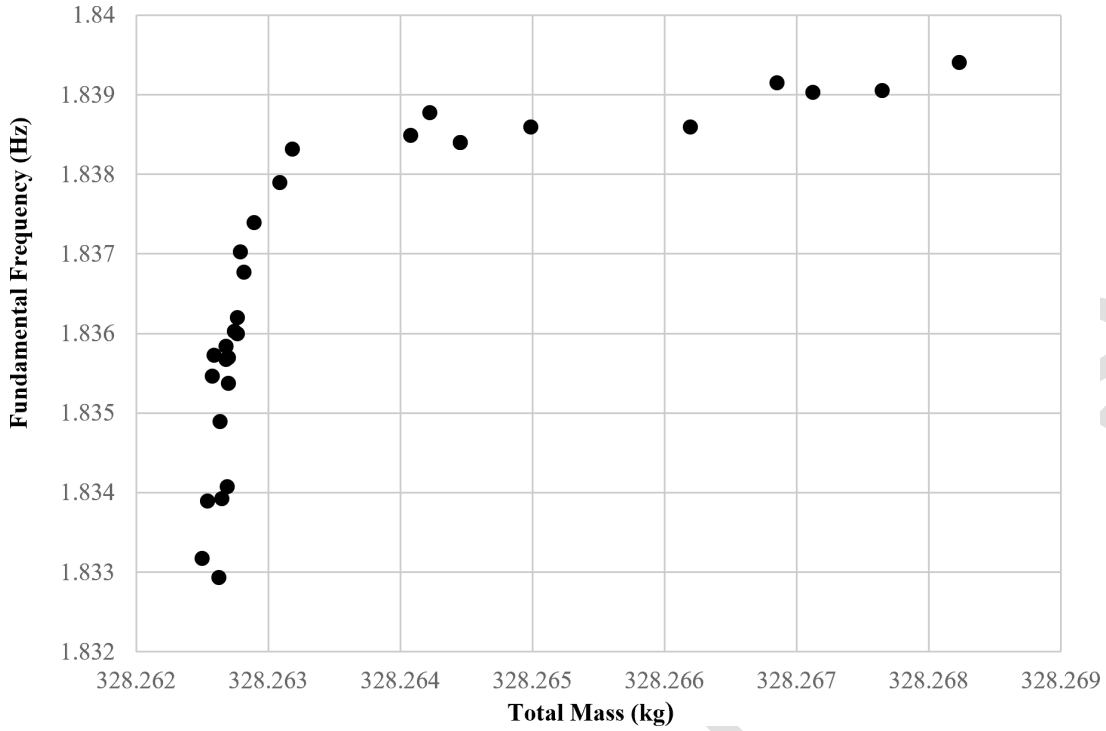

Fig. 9. Pareto front: mass-frequency optimization trade-off

fundamental frequency is increased by 9.12 % (from 1.6699 Hz to 1.8375 Hz). This simultaneous improvement of both objectives is made possible by a redistribution of material properties: a reduction in the composite density is compensated for by an increase in its Young's modulus and the aerodynamic operating conditions are slightly adjusted. This solution respects the structural constraints, with deformation and equivalent stress levels maintained within safe limits, thereby validating the robustness of the optimized design.

To confirm the robustness and accuracy of the MOGA optimization framework, the optimal candidate point selected from the Pareto front was subjected to an independent numerical re-verification analysis. This was achieved by running a direct, high-fidelity co-simulation (CFD-FEA) in ANSYS using the optimized design variables.

Table 6. Comparison of original and optimized design parameters and performance

Parameters	Original design	Optimized solution
Fluid density [kg/m^3]	1.225	1.2422
Flow velocity [m/s]	12	11.986
Rotational speed [rad/s]	2.22	2.4128
Material density [kg/m^3]	1 550	1 395
Young's modulus X [Pa]	1.1375×10^{11}	1.2503×10^{11}
Max. total deformation [m]	0.5643	0.56565
Max. equivalent stress [Pa]	3.8756×10^{7}	4.2911×10^{7}
Total mass [kg]	364.7361	328.2644
Fundamental frequency [Hz]	1.6699	1.8375

Table 7. Model validation: comparison between Kriging-MOGA predictions and numerical verification

Parameters	Optimized solution (Kriging-MOGA)	Verified solution (Direct ANSYS)	Deviation
Max. total deformation [m]	0.56565	0.56454	$0.20\,\%$
Max. equivalent stress [Pa]	4.2911×10^7	4.2859×10^7	$0.12\,\%$
Total mass [kg]	328.2644	328.2644	$0.00\,\%$
Fundamental frequency [Hz]	1.8375	1.8376	$0.01\,\%$

Table 7 compares the values predicted by the surrogate model with the direct numerical verification results. The differences are negligible (below 0.2 % across all structural and aerodynamic criteria), definitively attesting to the high reliability of the Kriging metamodel and the robustness of MOGA.

6. Conclusion

The conducted optimization study on the wind turbine blade, considering FSI analysis, confirmed the effectiveness of the implemented multi-step methodology. This work leveraged the coupling of numerical tools, utilizing ANSYS Mechanical and ANSYS Fluent for the FSI modeling and simulation and MATLAB/Simulink for the optimization analysis. The approach began with a sensitivity analysis to identify influential parameters and a LHS experimental design (sized using the empirical rule of $N = 10k$) was implemented to efficiently explore the design space. The constructed Kriging metamodel demonstrated high predictive capability, enabling the establishment of an accurate response surface for the optimization phase. The study achieved its primary objective by identifying the complete set of optimal compromise solutions for blade design, aiming to minimize total mass while maximizing the fundamental frequency under strict constraints. The application of MOGA to this metamodel enabled the generation of a robust Pareto front, mapping all non-dominated solutions with significant improvement over the original design by reducing approximately 10 % of the total mass and increasing the fundamental frequency by approximately 9 %. The accuracy of the surrogate framework was formally validated through an independent check in ANSYS. The deviations between the LHS-Kriging-MOGA predictions and the direct simulation results were negligible (below 0.2 %). Furthermore, this cross-validation ensures that the optimal candidate design represents a fully feasible solution, strictly satisfying all structural limits for maximum deformation and equivalent stress.

The originality of this work lies in the implementation of an automated computational chain integrating high-fidelity FSI simulations within a metamodel-based optimization process. This approach overcomes the prohibitive computational cost of direct simulations while preserving the accuracy required for the analysis of large-scale structures. The major advantage of this methodology resides in its capacity to explore a vast and non-linear design space, thus offering a robust tool for the preliminary design of wind turbine blades where fluid-structure interactions are predominant.

References

[1] Abdoulaye, H. I., El Maani, R., Numerical simulation of fluid–structure interaction in wind turbines: A reduced-order approach via periodic modeling and substructuring, Applied Mechanics 7 (1) (2026) No. 1. https://doi.org/10.3390/applmech7010001

[2] Afzal, A., Kim, K.-Y., Seo, J.-W., Effects of Latin hypercube sampling on surrogate modeling and optimization, International Journal of Fluid Machinery and Systems 10 (3) (2017) 240–253. https://doi.org/10.5293/IJFMS.2017.10.3.240

[3] ANSYS, Inc., ANSYS DesignXplorer User's Guide, Release 2025, Canonsburg, PA, USA.

[4] Batay, S., Baidullayeva, A., Zhao, Y., Wei, D., Baigarina, A., Sarsenov, E., Shabdan, Y., Aerostructural design optimization of wind turbine blades, Processes 12 (1) (2024) No. 22. https://doi.org/10.3390/pr12010022

[5] Bhaskaran, R., CornellX: A hands-on introduction to engineering simulations, Online course, Cornell University. https://www.edx.org/course/a-hands-on-introduction-to-engineering-simulations

[6] Couto, L. L., Moreira, N. E., Saito, J. Y. O., Hallak, P. H., Lemonge, A. C. C., Multi-objective structural optimization of a composite wind turbine blade considering natural frequencies of vibration and global stability, Energies 16 (8) (2023) No. 3363. https://doi.org/10.3390/en16083363

[7] El Maani, R., Radi, B., El Hami, A., Multiobjective backtracking search algorithm: Application to FSI, Structural and Multidisciplinary Optimization 59 (1) (2019) 131–151. https://doi.org/10.1007/s00158-018-2056-6

[8] El Maani, R., Radi, B., El Hami, A., Numerical study and optimization-based sensitivity analysis of a vertical-axis wind turbine, Energies 17 (24) (2024) No. 6300. https://doi.org/10.3390/en17246300

[9] Forrester, A. I. J., Sóbester, A., Keane, A. J., Engineering design via surrogate modelling: A practical guide, Chichester, John Wiley & Sons, 2008. https://doi.org/10.1002/9780470770801

[10] Gutmann, H.-M., A radial basis function method for global optimization, Journal of Global Optimization 19 (3) (2001) 201–227. https://doi.org/10.1023/A:1011255519438

[11] He, F., Zheng, X., Luo, W., Zhong, J., Huang, Y., Ye, A., Qiu, R., Ma, H., Collaborative optimization of aerodynamics and wind turbine blades, Applied Sciences 15 (2) (2025) No. 834. https://doi.org/10.3390/app15020834

[12] Jones, D. R., Schonlau, M., Welch, W. J., Efficient global optimization of expensive black-box functions, Journal of Global Optimization 13 (4) (1998) 455–492. https://doi.org/10.1023/A:1008306431147

[13] Konak, A., Coit, D. W., Smith, A. E., Multi-objective optimization using genetic algorithms: A tutorial, Reliability Engineering & System Safety 91 (9) (2006) 992–1 007. https://doi.org/10.1016/j.ress.2005.11.018

[14] Li, L., Zhang, W., Li, Y., Jiang, C., Wang, Y., Multi-objective optimization of turbine blade profiles based on multi-agent reinforcement learning, Energy Conversion and Management 197 (2023) No. 117637. https://doi.org/10.1016/j.enconman.2023.117637

[15] Loeppky, J. L., Sacks, J., Welch, W. J., Choosing the sample size of a computer experiment: A practical guide, Technometrics 51 (4) (2009) 366–376. https://doi.org/10.1198/TECH.2009.08040

[16] Moustapha, M., Sudret, B., Bourinet, J.-M., Guillaume, B., Quantile-based optimization under uncertainties using adaptive Kriging surrogate models, Structural and Multidisciplinary Optimization 54 (6) (2016) 1 403–1 421. https://doi.org/10.1007/s00158-016-1504-4

[17] Regis, R. G., Shoemaker, C. A., A stochastic radial basis function method for the global optimization of expensive functions, INFORMS Journal on Computing 19 (4) (2007) 497–509. https://doi.org/10.1287/ijoc.1060.0182

[18] Thapa, M., Missoum, S., Uncertainty quantification and global sensitivity analysis of composite wind turbine blades, Reliability Engineering & System Safety 222 (2022) No. 108354. https://doi.org/10.1016/j.ress.2022.108354

[19] Wang, G. G., Shan, S., Review of metamodeling techniques in support of engineering design optimization, Journal of Mechanical Design 129 (4) (2007) 370–380. https://doi.org/10.1115/1.2429697